World Journal of

Gastrointestinal Oncology

World Journal of Gastrointestinal Oncology

Contents

Monthly Volume 15 Number 5 May 15, 2023

Contents

Contents

ABOUT COVER

Editorial Board Member of *World Journal of Gastrointestinal Oncology*, Claudio Luchini, MD, PhD, Associate Professor of Pathology, Department of Diagnostics and Public Health, University and Hospital Trust of Verona, Verona 37134, Italy. claudio.luchini@univr.it

AIMS AND SCOPE

The primary aim of *World Journal of Gastrointestinal Oncology* (*WJGO, World J Gastrointest Oncol*) is to provide scholars and readers from various fields of gastrointestinal oncology with a platform to publish high-quality basic and clinical research articles and communicate their research findings online.

WJGO mainly publishes articles reporting research results and findings obtained in the field of gastrointestinal oncology and covering a wide range of topics including liver cell adenoma, gastric neoplasms, appendiceal neoplasms, biliary tract neoplasms, hepatocellular carcinoma, pancreatic carcinoma, cecal neoplasms, colonic neoplasms, colorectal neoplasms, duodenal neoplasms, esophageal neoplasms, gallbladder neoplasms, *etc*.

INDEXING/ABSTRACTING

The *WJGO* is now abstracted and indexed in PubMed, PubMed Central, Science Citation Index Expanded (SCIE, also known as SciSearch®), Journal Citation Reports/Science Edition, Scopus, Reference Citation Analysis, China National Knowledge Infrastructure, China Science and Technology Journal Database, and Superstar Journals Database. The 2022 edition of Journal Citation Reports® cites the 2021 impact factor (IF) for *WJGO* as 3.404; IF without journal self cites: 3.357; 5-year IF: 3.250; Journal Citation Indicator: 0.53; Ranking: 162 among 245 journals in oncology; Quartile category: Q3; Ranking: 59 among 93 journals in gastroenterology and hepatology; and Quartile category: Q3. The *WJGO*'s CiteScore for 2021 is 3.6 and Scopus CiteScore rank 2021: Gastroenterology is 72/149; Oncology is 203/360.

RESPONSIBLE EDITORS FOR THIS ISSUE

ORIGINAL ARTICLE

Basic Study

BZD9L1 benzimidazole analogue hampers colorectal tumor progression by impeding angiogenesis

Chern Ein Oon, Ayappa V Subramaniam, Lik Yang Ooi, Ashwaq Hamid Salem Yehya, Yeuan Ting Lee, Gurjeet Kaur, Sreenivasan Sasidharan, Beiying Qiu, Xiaomeng Wang

Chern Ein Oon, Ayappa V Subramaniam, Lik Yang Ooi, Yeuan Ting Lee, Gurjeet Kaur, Sreenivasan Sasidharan, Institute for Research in Molecular Medicine, Universiti Sains Malaysia, Penang 11800, Malaysia

Ashwaq Hamid Salem Yehya, Cancer Research, Eman Biodiscoveries, Kedah 08000, Malaysia

Ashwaq Hamid Salem Yehya, Vatche and Tamar Division of Digestive Diseases, Department of Medicine, David Geffen School of Medicine at University of California Los Angeles, Los Angeles, CA 90095, United States

Beiying Qiu, Xiaomeng Wang, Academic Clinical Program, Duke-NUS Medical School, National University of Singapore, Singapore 169857, Singapore

Beiying Qiu, Singapore National Eye Centre, Singapore Eye Research Institute, Singapore 168751, Singapore

Xiaomeng Wang, Singapore National Eye Centre, Singapore Eye Research Institute, Singapore 169857, Singapore

Corresponding author: Chern Ein Oon, DPhil, PhD, Associate Professor, Institute for Research in Molecular Medicine, Universiti Sains Malaysia, Gelugor, Penang 11800, Malaysia. chern.oon@usm.my

Abstract

BACKGROUND
The development of new vasculatures (angiogenesis) is indispensable in supplying oxygen and nutrients to fuel tumor growth. Epigenetic dysregulation in the tumor vasculature is critical to colorectal cancer (CRC) progression. Sirtuin (SIRT) enzymes are highly expressed in blood vessels. BZD9L1 benzimidazole analogue is a SIRT 1 and 2 inhibitor with reported anticancer activities in CRC. However, its role has yet to be explored in CRC tumor angiogenesis.

AIM
To investigate the anti-angiogenic potential of BZD9L1 on endothelial cells (EC) *in vitro*, *ex vivo* and in HCT116 CRC xenograft *in vivo* models.

METHODS

EA.hy926 EC were treated with half inhibitory concentration (IC_{50}) (2.5 μM), IC_{50} (5.0 μM), and double IC_{50} (10.0 μM) of BZD9L1 and assessed for cell proliferation, adhesion and SIRT 1 and 2 protein expression. Next, 2.5 μM and 5.0 μM of BZD9L1 were employed in downstream *in vitro* assays, including cell cycle, cell death and sprouting in EC. The effect of BZD9L1 on cell adhesion molecules and SIRT 1 and 2 were assessed *via* real-time quantitative polymerase chain reaction (qPCR). The growth factors secreted by EC post-treatment were evaluated using the Quantibody Human Angiogenesis Array. Indirect co-culture with HCT116 CRC cells was performed to investigate the impact of growth factors modulated by BZD9L1-treated EC on CRC. The effect of BZD9L1 on sprouting impediment and vessel regression was determined using mouse choroids. HCT116 cells were also injected subcutaneously into nude mice and analyzed for the outcome of BZD9L1 on tumor necrosis, Ki67 protein expression indicative of proliferation, cluster of differentiation 31 (CD31) and CD34 EC markers, and SIRT 1 and 2 genes *via* hematoxylin and eosin, immunohistochemistry and qPCR, respectively.

RESULTS
BZD9L1 impeded EC proliferation, adhesion, and spheroid sprouting through the downregulation of intercellular adhesion molecule 1, vascular endothelial cadherin, integrin-alpha V, SIRT1 and SIRT2 genes. The compound also arrested the cells at G1 phase and induced apoptosis in the EC. In mouse choroids, BZD9L1 inhibited sprouting and regressed sprouting vessels compared to the negative control. Compared to the negative control, the compound also reduced the protein levels of angiogenin, basic fibroblast growth factor, platelet-derived growth factor and placental growth factor, which then inhibited HCT116 CRC spheroid invasion in co-culture. In addition, a significant reduction in CRC tumor growth was noted alongside the downregulation of human SIRT1 (hSIRT1), hSIRT2, CD31, and CD34 EC markers and murine SIRT2 gene, while the murine SIRT1 gene remained unaffected, compared to vehicle control. Histology analyses revealed that BZD9L1 at low (50 mg/kg) and high (250 mg/kg) doses reduced Ki-67 protein expression, while BZD9L1 at the high dose diminished tumor necrosis compared to vehicle control.

CONCLUSION
These results highlighted the anti-angiogenic potential of BZD9L1 to reduce CRC tumor progression. Furthermore, together with previous anticancer findings, this study provides valuable insights into the potential of BZD9L1 to co-target CRC tumor vasculatures and cancer cells *via* SIRT1 and/or SIRT2 down-regulation to improve the therapeutic outcome.

Core Tip: BZD9L1 hampered EA.hy926 endothelial cell functions through cell cycle arrest and induction of apoptosis. BZD9L1 also reduced the cell adhesion, sirtuin 1 (SIRT1) and SIRT2 gene expression in endothelial cells (EC) compared to the negative control. The compound down-regulated angiogenin, basic fibroblast growth factor, platelet-derived growth factor, and placental growth factor proteins in EC and impeded HCT116 colorectal cancer (CRC) invasion compared to the negative control group. BZD9L1 negatively impacted choroidal sprouting and CRC tumor angiogenesis *in vivo* compared to the vehicle control group. BZD9L1 reduced tumor necrosis, Ki-67 proliferation marker, hSIRT1, hSIRT2, murine cluster of differentiation 31 (mCD31), mCD34 and murine SIRT2 (mSIRT2) gene expression compared to vehicle control. Findings from this study may provide insights for the BZD9L1 benzimidazole analogue to be further explored as a potential anti-angiogenic agent in CRC.

INTRODUCTION

Cancer may arise from genetic or epigenetic dysregulations. Many conventional therapies focus on removing and disrupting malignant cells but fail to target the tumor microenvironment, which could

fuel tumor growth through pathway crosstalks and the secretion of cytokines. Epigenetic dysregulation has been shown to stimulate oncogenic transformation in many cancer types, including colorectal cancer (CRC). Furthermore, research has highlighted the importance of epigenetic regulation in angiogenesis, which is key to CRC growth and metastasis. Advancements in therapeutic care for CRC patients have identified various angiogenesis inhibitors targeting the tyrosine kinases and vascular endothelial growth factor (VEGF) proteins used in clinics. However, some patients are resilient or have become less susceptible to these anti-angiogenic drugs[1], possibly due to dynamic host response factors or mutations within tumors that render drug insensitivity. Therefore, there is a need to uncover alternative targeted therapies. Sirtuins (SIRT 1-7) are nicotinamide adenine dinucleotide (NAD+) -dependent class III histone deacetylases. Their potential roles through epigenetic modulation in cancer have stimulated investigation to seek potent and selective SIRT inhibitors, potentially leading to new therapeutic breakthroughs.

Benzimidazole derivatives have been widely used in other areas, such as antiviral[2] and anti-mycobacterial[3] agents; hence their pharmacokinetics are well understood. The discovery of indole analogues as potent sirtuin inhibitors[4] and the high similarities between the indole and benzimidazole core structures have led to the discovery of BZD9L1[5] and its reported anticancer activities as a single agent[6] or in combination with 5-fluorouracil in CRC[7]. However, to our knowledge, no known sirtuin inhibitors have been studied concerning their application to modulate angiogenesis. Hence, this study opens a new avenue for developing a prospective anti-angiogenic agent (BZD9L1) through sirtuin inhibition in CRC.

MATERIALS AND METHODS

Cells and cell culture

The Ea. hy926 endothelial cells (EC) and the HCT-116 CRC cell line were purchased from American Type Culture Collection (ATCC®). The cells were maintained in Dulbecco's Modified Eagle Medium (DMEM) and Roswell Park Memorial Institute (RPMI), respectively (Thermo Scientific, United States), supplemented with 5% fetal bovine serum (Biowest, United States), 1% penicillin-streptomycin (Nacalai Tesque, United States). Cells were kept at 37°C in a humidified incubator with 5% CO_2 atmosphere.

Treatments

BZD9L1 was synthesized as previously described[5]. BZD9L1 was prepared and dissolved in dimethyl sulfoxide (DMSO) (Nacalai Tesque, United States) for *in vitro* and *ex vivo* evaluations. Different concentrations of BZD9L1 and anti-angiogenic agents Sunitinib (AdooQ Bioscience, CA, United States)[8] or activin A receptor like type 1 (ALK1) inhibitor (Axon MedChem)[9] positive controls were used to treat the cells according to assay requirements. For animal administration, BZD9L1 was prepared in 0.5% sodium carboxymethyl cellulose (CMC) solution as previously reported[10] and administered to the rodents *via* intraperitoneal injection, in which 0.5% CMC was also employed as the vehicle control *in vivo*.

Animals for in vivo study

The animal study was approved and conducted in strict accordance with Universiti Sains Malaysia Animal Ethical Committee [No. USM/IACUC/2017/(105)(872)]. Male and female athymic nude mice were procured from EMAN Biodiscoveries Sdn. Bhd. The mice were maintained in filter-top cages under controlled atmospheric conditions at Natureceuticals Sdn Bhd, Kawasan Perindustrian Sungai Petani, Sungai Petani, Kedah. The mice were 4-6 wk of age with a body weight of 18-20 g. The mice were provided with autoclaved food and water. The bedding was refreshed every 48 h.

Animals for ex vivo study

Male and female C57BL/6J mice were sourced from Invivos (Singapore) and retained on a 12 h light-dark cycle. The mice were fed a standard rodent chow (NCD, 18% kcal from fat, Harlan). The *ex vivo* assays, which require the choroids from the mice, were performed in compliance with the National University of Singapore Institutional Animal Care and Use Committee guidelines (IACUC) (No. 2020/SHS/1597).

Cell viability assay

The 3-(4,5-dimethylthiazol-2-yl)-2,5 diphenyl tetrazolium bromide (MTT) cell viability assay was performed to determine half inhibitory concentration (IC_{50}) and suitable dosage of BZD9L1. MTT reagent diluted with phosphate-buffered saline (PBS) at 5 mg/mL was used for the MTT assay. Cells (2.5×10^3) were seeded in 96-well plates with 100 μL of compatible media per well and incubated in 5% CO_2 at 37 °C for 24 h. Different doses of BZD9L1 (0 μM, 1.560 μM, 3.125 μM, 6.250 μM, 12.500 μM, 25.000 μM, 50.000 μM, and 100.000 μM) were tested on Ea.hy926 cells to select the best cytotoxic concentrations and then incubated in 5% CO_2 at 37 °C. After 72 h, 20 μL of MTT reagent per well was added and then

incubated in 5% CO_2 at 37 ℃ for 4. Next, the supernatant was carefully aspirated and 200 μL of DMSO added. After gently shaking the plate, the mixture's optical density (OD) was measured using a microplate reader (TECAN, Switzerland) at 570 nm primary and 620 nm reference wavelength. The percentage of viable cells at each treatment concentration was calculated using the following equation: Cell viability (%) = (absorbance of samples/absorbance of vehicle control) × 100%.

xCELLigence cell adhesion assay

The effect of BZD9L1 towards cell adhesion was determined using the xCELLigence Real-Time Cell Analysis (RTCA) instrument (Agilent Technologies, United States) according to the standard manufacturer's protocol. Briefly, the cells were resuspended in treatment media conditions: Vehicle control, 2.5 μM, 5.0 μM, and 10.0 μM of BZD9L1. Then, the cells and treatment media were seeded into the E96 xCELLigence plate at 1×10^4 cells per well. The E-96 xCELLigence plate was incubated for 30 min at room temperature and placed on the xCELLigence station in the cell culture incubator. The cellular impedance was continuously monitored every 30 min for 5 h. Impedance recordings from each well in the E96 xCELLigence plate were automatically converted to cell index (CI) values by the xCELLigence RTCA software.

xCELLigence cell proliferation assay

Real-time analysis of EA.hy926 cell proliferation was evaluated using the xCELLigence RTCA instrument (Agilent Technologies, United States). Firstly, 100 μL of growth media was added to each well of an E96 xCELLigence plate. The plate was then inserted into the xCELLigence station. Next, baseline impedance measurement was performed to obtain background readings. EA.hy926 cells were harvested and adjusted to 1×10^4 cells per well. The cells were resuspended in 100 μL of media and seeded into the E96 xCELLigence plate. E-96 xCELLigence plate containing cells was incubated for 30 min at room temperature and placed on the xCELLigence station in the cell culture incubator. After 24 h, treatment comprising of vehicle control, BZD9L1 at 2.5 μM, 5.0 μM, and 10.0 μM were introduced to the cells in the plate, then returned to the xCELLigence station in an incubator for continuous impedance recording. Cell proliferation was monitored every 30 min for 72 h. Measured impedance recordings from cells in each well on the E96 xCELLigence plate were automatically converted to Cell Index (CI) values by the xCELLigence RTCA software.

Cell cycle analysis

The cell cycle analysis was performed to differentiate different cell cycle phases that were arrested after the treatments above. On day 0, Ea.hy926 cells were seeded in a T25 culture flask at a concentration of 5×10^5 per flask. Each treatment group was assigned a flask. The cells were incubated at 37 ℃ in a humidified atmosphere of 5% (v/v) CO_2 to promote cell attachment. The next day, the medium was meticulously removed and replaced with fresh medium containing treatments and then incubated for 72 h at 37 ℃ in a humidified atmosphere of 5% (v/v) CO_2. After 72 h, the cells were collected, centrifuged, and fixed with 70% ethanol (molecular grade) at 4 ℃. Finally, the fixed cells were stained with 500 μL of warm propidium iodide (PI) solution plus 50 μL of RNase A stock solution (1 mg/mL). The cells were incubated in the dark for 30 min. The stained cells were kept on ice until the scheduled flow cytometry analysis using BD FACSCalibur (BD Biosciences, United States).

Apoptosis detection

Apoptotic cells were detected by flow cytometry using Annexin V-fluorescein isothiocyanate (FITC) Apoptosis Detection Kit (Elabscience, China). On day 0, Ea. hy926 cells were seeded in a T25 culture flask at a concentration of 5×10^5 per flask. Each treatment group was assigned a flask. The cells were incubated at 37 ℃ in a humidified atmosphere of 5% (v/v) CO_2 to promote cell attachment. The next day, the medium was meticulously removed and replaced with fresh medium containing treatments before incubation for 72 h at 37 ℃ in a humidified atmosphere of 5% (v/v) CO_2. After 72 h, the cells were harvested and centrifuged, and the cell concentration was adjusted to 1×10^6 for each tube. The Annexin V-FITC Apoptosis Detection Kit was used to stain the cells, and cell apoptosis was determined by flow cytometry, according to the manufacturer's instruction. The tubes were incubated at room temperature for 15 min in the dark, after which the cells were subjected to flow cytometry analysis immediately using BD FACSCalibur (BD Biosciences, United States) using 488 nm excitation and 525 nm emission for FITC and 655-730 nm emission for PI.

Hanging drop spheroid formation and sprouting assay

The 3-dimensional spheroid sprouting assay mimics the *in vivo* microenvironment of tissue or tumors. Hanging drop spheroid formation and sprouting assay was conducted to provide a three-dimensional aspect to both architecture and share the limited drug penetration properties since drugs are primarily confined to the outer cell layers. Culturing cells in three dimensions is much more representative of the *in vivo* environment than traditional two-dimensional cultures. In this present study, Ea.hy 926 was used to generate micro-spheroids. After trypsinization of cultured cells, the cells were harvested and resuspended in DMEM medium containing 0.25% methylcellulose. Drops (20 μL) of medium containing

2×10^3 cells were seeded onto the lids of 100 mm petri dishes, and the dishes were supplied with 5 mL of PBS to maintain humidity. The drops were incubated for 72 h to encourage the occurrence formation of spheroids. Treatments were prepared at different concentrations of BZD9L1 (2.5 µM and 5.0 µM) and sunitinib (18 µM) as a positive control in media and then added to each well. The resulting aggregate cells (spheroids) were harvested carefully using 200 µL pipettes and then introduced into a 96-well plate precoated with 50 µL matrigel per well. The plate was left to incubate in the incubator at 37 ℃, and pictures were taken using a phase contrast microscope (Zeiss, Germany) on days 0 and 3. The length of the sprouts was measured and analyzed as previously described[11] using Image J (Fiji).

Angiogenesis array

The Quantibody Human Angiogenesis Array (RayBiotech, Inc, Norcross, GA) was used to determine the concentration of ten proangiogenic cytokines [angiogenin, angiopoietin-2, epidermal growth factor (EGF), basic fibroblast growth factor (bFGF), heparin-binding EGF, hepatocyte growth factor, leptin, platelet-derived growth factor (PDGF-BB), placental growth factor (PIGF), and VEGF-A]] secreted by the EC. Each cytokine was arrayed in quadruplicate, together with positive and negative controls. In addition, one standard glass slide was divided into 16 wells of identical cytokine antibody array. Approximately 2.5×10^3 of Ea. hy926 cells were seeded in 96-well plates with 100 µL of compatible media per well and incubated in 5% CO_2 at 37 ℃ for 24 h. The next day, vehicle control, 2.5 µM, and 5.0 µM of BZD9L1 treatment were prepared using 1% serum media and introduced to the cells. After 48 h, the media was discarded, and the cells were washed with 1 × PBS twice before reintroducing serum-free media. After another 48 h, the conditioned media was collected. The conditioned media was used on the angiogenesis antibody array kit (Quantibody Human Angiogenesis Array 1) as per manufacturer's instructions. The slides were mailed to RayBiotech testing services (Singapore) for laser scanning analysis. Data were extracted and analyzed using the RayBio Q Analyzer software (RayBiotech, Inc).

RNA extraction

Total cellular RNA was extracted from EA.hy926 cells treated with vehicle control (DMSO) or different concentrations of BZD9L1 at 4 h time point, or HCT116 xenograft tumors post-treatment, using GENEZOL (Geneaid, New Taipei City, Taiwan) according to the manufacturer's instructions. Firstly, the spent medium was discharged from each well and the cells were rinsed with 1 × PBS twice. Next, 1 mL of GENEZOL reagent solution was added to each well. The cells were lysed *via* repeated pipetting and followed by 10 min of incubation at room temperature for sample homogenization. The lysed cells were then transferred into 2 mL microcentrifuge tubes. An accurate amount of 200 µL chloroform was added to each tube. Each tube was mixed thoroughly by vortexing for 15 s. The lysates were then centrifuged at 16000 g for 15 min at 4 ℃. The colourless upper aqueous phase was carefully transferred into a new 1.5 mL microcentrifuge tube without drawing any of the interphase or organic phase layer that appears white and red in the three-layers mixture respectively. Next, 1 to 1 volume of ice-cold isopropanol was added to the aqueous phase. The 1.5 mL tubes were inverted several times for proper mixing, followed by 10 min of incubation at room temperature. The tubes were centrifuged at 16000 × g for 10 min at 4 ℃ to form a tight RNA pellet. The supernatant was removed completely, and the pellet was resuspended with 1 mL 75% ethanol. The mixture was vortexed briefly and centrifuged again at 16000 g at 4 ℃ for 5 min to remove all traces of ethanol. The supernatant was carefully removed by using a pipette tip, and the pellet was allowed to air dry for 15 min. After 15 min of air drying, the pellet was resuspended with 20 µL DEPC-treated water and incubated at 60 ℃ for 15 min to dissolve the RNA pellet. RNA was then converted to cDNA or immediately stored at -80 ℃ freezer until further use. The purity and concentration of the isolated RNA were determined by measuring the optical density at 260 nm and 260/280 nm ratio using a NanoDrop 2000 spectrophotometer (Thermo Scientific, Pennsylvania, United States). A preset of 40 ng/µL per OD was used with a baseline correction of 340 nm.

Quantitative polymerase chain reaction

The RNA was reverse transcribed into cDNA using Tetro cDNA Synthesis Kit (Bioline, United States) according to the manufacturer's protocol. Real-time quantitative polymerase chain reaction (qPCR) was performed using the KAPA SYBR FAST qPCR Kit Master Mix (2 ×) Universal (Biosystems, United States) with the following conditions: denaturation, 95 ℃ for 20 s; annealing, 58 ℃, 20 s and extension, 68 ℃, 30 s. All samples were tested in triplicate PCR reactions, and the mean of the reactions was used for calculating the expression levels. All the data were collected from the linear range of each amplification. Two housekeeping genes (HKGs) were used to normalize the expression of genes of interest (GOIs). Expression levels of GOIs were normalized to glyceraldehyde 3-phosphate dehydro-genase (GAPDH) and human 18S ribosomal RNA (18S rRNA) gene for human targets, and mouse 18S ribosomal RNA (m18S rRNA) and mouse Peptidylprolyl isomerase A (mPpia) genes for mouse targets. The data were analyzed using the comparative CT (ΔΔCT) method, where the expression value of the GOI was normalized to the respective HKG. The change of gene expression was determined by setting the expression value of vehicle control sample to 1, and expression values of GOI were compared where values < 1 represented downregulation and values > 1 represented upregulation of that particular GOI. The final results were reported as mean ± SEM to reflect the triplicate measurements. The list of primers

used for qPCR analysis is listed in Table 1.

Ex vivo mouse choroid microvascular assay

Organotypic cultures are *in vitro* growth of 3D biological tissues that closely emulate part of their natural function and physiology. Choroid sprouting assay was performed as described[12]. C57BL/6J mice were killed by cervical dislocation. The choroid explants from post-natal day 3 C57BL/6J mice were isolated through a very tedious process under a stereo microscope. Briefly, the cornea and lens were removed from the anterior of the eye, followed by the separation of the peripheral choroid-sclera complex from the retina. The choroid was then cut into 1mm × 1mm segments. The choroid explants were then incubated in reduced growth factor Matrigel (BD Biosciences). Vascular outgrowth, including cells from the microenvironment from the choroidal tissues treated with DMSO vehicle control, BZD9L1 at 10 µM and 20 µM or ALK1 inhibitor (Axon MedChem) at 100 nM. After 96 h, the effect of BZD9L1 on the morphological changes of vessel sprouts was noted. The regression study performed as previously reported[13], in which treatment media containing either DMSO (negative control), BZD9L1 at concentrations of 10 µM and 20 µM or ALK1 inhibitor at 50 nM were added to the explants on day 2 when the embedded choroids had sprouted. Media were changed every other day. Images were taken 24 h post-treatment. Imaging and quantifying the sprouting area were performed under the Eclipse Ti-E Inverted Research Microscope (Nikon, Tokyo, Japan). and TRI2 software (version: 3.0.1.2, TRI2, Oxford, United Kingdom).

Indirect co-culture assay

The co-culture assay was conducted to study the interaction between ECs and cancer cells. The application of a co-culture model promotes a better understanding of the dynamic tumor-EC relationship that occurs *in vivo* in an inexpensive and *in vitro* laboratory setting. In this study, the co-culture was conducted indirectly. Ea. hy926 and HCT116 cell lines were used in this experiment. Steps to collect conditioned media were repeated as per described for the angiogenesis array. The conditioned media can be used fresh or stored in a -80 °C freezer for later use. Treatments were prepared at different concentrations of BZD9L1 (2.5 µM and 5.0 µM) and sunitinib (18 µM) as a positive control. HCT 116 spheroids were prepared and introduced into the rat tail collagen mixed to a concentration of 1.6 mg/mL before mixing it with spheroid suspension, a spreviously described[7]. The mixture was dispensed at 400 uL in each well in a 24-well plate. The plate was incubated for 30 min before 500 µL of the conditioned media was introduced. The plate was left in the incubator at 37 °C, and pictures were taken using a phase contrast microscope (Zeiss, Germany) on days 0 and 3.

Tumor xenograft model

Xenograft models are based on the implantation of human tumor cells into genetically modified mice models that are immunocompromised to avoid graft *vs* host reaction of the mouse against the human tumor tissue. Male/female athymic nude mice (procured from EMAN Biodiscoveries Sdn. Bhd.) were maintained in filter-top cages under controlled atmospheric conditions. The mice were 4-6 wk of age with a body weight of 18-20 g. Mice were provided autoclaved food and water, and the bedding was changed every 48 h. HCT-116 cells at 90% confluency were harvested and injected subcutaneously onto the right dorsal flank of the animal at a density of 1×10^6 cells per 200 µL of media mixed with matrigel at a ratio of 1:1. The mice were then randomly divided into four groups (n = 6) and given different treatments, consisting of vehicle control, BZD9L1 at 50 mg/kg or 250 mg/kg and sunitinib at 40 mg/kg as the positive control[14], when at least three tumors reached 100 mm³. The treatments were diluted in 0.5% carboxymethylcellulose (CMC) solution. The control group was treated with 0.5% CMC only. The treatments were injected intraperitoneally at a maximum volume of 250 µL once every three days, alongside the measurement of weight and tumor size using the standard formula: Volume of tumor = π/6 × (length × width × height), as previously reported[7].

The animals were euthanized when the tumor reached the maximum size of 1000 mm³. The tumors were harvested and fixed in a 10% buffered formaldehyde solution and then processed by an automated tissue processing machine for histological examination. The HCT116 xenograft tumor samples were cut into small pieces using a sterile surgical blade for gene expression analyses. GENEZOL reagent was added to the tumor tissue sample and placed on ice. The tissue was then homogenized using a handheld homogenizer. The mixture was centrifuged at 13000 × g for 15 min at 4 °C to separate the phases. The upper aqueous phase was transferred to a new 2.0 mL microcentrifuge tube, followed by the RNA extraction protocol described above.

Hematoxylin & Eosin staining

The impact of BZD9L1 treatment on tumor necrosis affecting tumor growth was determined by establishing a necrotic score. First, the slides were deparaffinized by heating the slides in the oven at 60 °C for 10 min. The slides were then immersed in the following order: Xylene (twice), absolute ethanol (twice), 95% ethanol (twice), 70% ethanol (once) and lastly, in distilled water, for 5 min each. Next, the slides were stained with hematoxylin for 5 min and then washed with distilled water for another 5 min. The slides were later counterstained with eosin for 15 s. Finally, the slides were washed for 5 min and

Table 1 List of primers		
Genes	**Primer sequences**	
	Forward sequences (5' to 3')	**Reverse sequences (3' to 5')**
mPpia	GAGCTGTTTGCAGACAAAGTTC	CCCTGGCACATGAATCCTGG
m18SrRNA	GGACCAGAGCGAAAGCATTTGCC	TCAATCTCGGGTGGCTGAACGC
18S rRNA	CGGCTACCACATCCAAGGAA	GCTGGAATTACCGCGGCT
mCD31	CCAAAGCCAGTAGCATCATGGTC	GGATGGTGAAGTTGGCTACAGG
mCD34	CTTCCCCAACTGGCATACTGC	TCCAGAGCATTTGATTTCTCCC
GAPDH	TGAACGGGAAGCTCACTGG	TCCACCACCCTGTTGCTGTA
ICAM	CGACTGGACGAGAGGGATTG	TTATGACTGCGGCTGCTACC
VE-cadherin	CCCTTCTTCACCCAGACCAA	CCGGTCAAACTGCCCATACT
ITGA5	CGGGCCCCTGCACCAACAAG	CAGCTGTGGCCACCTGACGC
mSIRT 1	CGGCTACCGAGGTCCATATAC	CAGCTCAGGTGGAGGAATTGT
mSIRT 2	GAGCCGGACCGATTCAGAC	AGACGCTCCTTTTGGGAACC
SIRT 1	TCTAACTGGAGCTGGGGTGT	TGGGAAGTCTACAGCAAGGC
SIRT 2	GCCCTTTACCAACATGGCTG	TTCGTACAACACCCAGAGCG

ITGA5: Integrin-alpha V; GAPDH: Glyceraldehyde 3-phosphate dehydrogenase; SIRT: Sirtuin; ICAM: Intercellular adhesion molecule; VE-cadherin: Vascular endothelial cadherin; CD31: Cluster of differentiation 31.

air-dried before being mounted.

Immunohistochemistry
The effect of BZD9L1 on proliferation was ascertained through Ki67 protein expression analysis on the xenograft tumor sections. The formalin fixed paraffin embedded slides were deparaffinized by heating the slides in an oven at 60 ℃ for 10 min. The slides were then immersed in the following order: absolute ethanol (twice), 95% ethanol (twice), 70% ethanol (once), followed lastly in distilled water for 5 min each. This procedure was carried out using the Dako Envision FLEX Kit. The sections were incubated in High pH antigen retrieval buffer (Dako) for 30 min. Next, the slides were washed with the wash buffer three times, for 5 min each. A few drops of Envision FLEX Peroxidase solution were introduced to the tissue for 10 min. The sections were then incubated with primary antibody Ki67 (Dako, Clone MIB-1, Cat#M7240, mouse monoclonal) and incubated at 4 ℃ overnight at 1:50 dilution. On the next day, the sections were rinsed in TBST and incubated with goat anti-mouse IgG secondary antibody for 1 h at 1:500 dilution, rinsed three times in TBST and followed by incubation with Dako® DAB solution. The slides were counterstained with hematoxylin for 5 min and then rinsed off before being mounted with glycerol (Sigma) and examined under a light microscope (CX41, Olympus). The Ki-67 score was established as the percentage of tumor cells positive for brown nuclear staining over the total number of nuclei from five random fields per tumor section.

Statistical analysis
GraphPad Prism 9.4.0 (GraphPad, United States) and Microsoft Excel (Microsoft, United States) were used for statistical analysis. The analysis of variance (One-way ANOVA) test was employed to compare mean values among three or more data sets, and Bonferroni post-test was employed to compare any two data sets among the three or more sets. Statistical significance was indicated in the figures, where [a]P < 0.05, [b]P < 0.01, and [c]P < 0.001, compared to the negative control or vehicle control. The non-regression curve was used to track the change in the tumor size and mouse body weight over time. Error bars represent the SEM.

RESULTS

BZDL1 reduced the viability and adhesion of Ea.HY926 cells
The effects of BZD9L1 on cell viability were assessed with MTT assay at 72 h. The half- IC_{50} of BZD9L1 in Ea HY926 was established to be at 5.2 μm (Figure 1A). BZD9L1 at 10 μM reduced the ability of the EC in suspension to adhere to the microtiter plates (E-Plates®) at 5 h (Figure 1B). BZD9L1 at 2.5 μM and 5.0

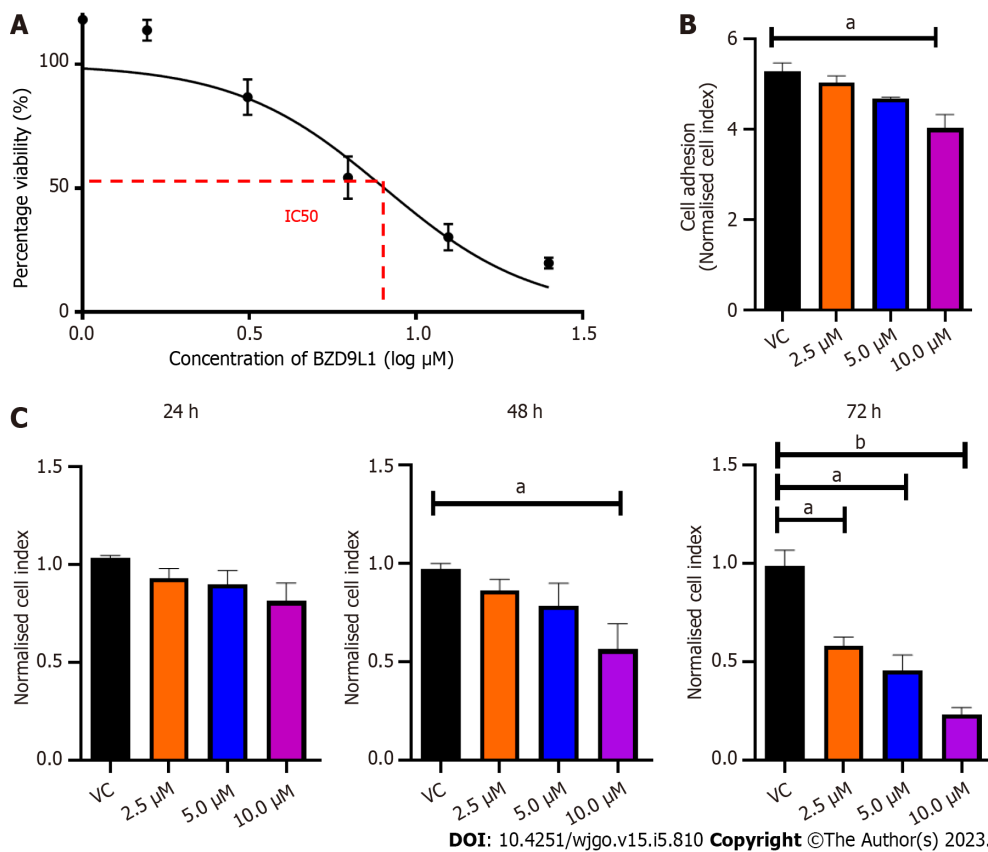**DOI**: 10.4251/wjgo.v15.i5.810 **Copyright** ©The Author(s) 2023.

Figure 1 Cell viability and adhesion analyses of Ea.HY926 endothelial cells treated with different concentrations of BZD9L1. A: Cell viability was determined using the MTT assay. The inhibitory concentration of BZD9L1 in Ea HY926 is 5.20 µm ± 0.38 µm (*n* = 3) at 72 h; B: Real-time xCELLigence impedance analysis of the area under the curve of BZD9L1-treated Ea.HY926 cells in suspension over 5 h. BZD9L1 at 10 µM reduced the ability of the endothelial cells to adhere to the microtiter plates (E-Plates®); C: Real-time xCELLigence impedance analysis of normalized cell index of BZD9L1-treated Ea.HY926 cells over 72 h. BZD9L1 at 2.5 µM and 5.0 µM had no significant impact on cell proliferation at 24 h and 48 h. Statistical analysis ([a]$P < 0.05$; [b]$P < 0.01$), one-way ANOVA with Bonferroni posthoc test, *n* = 3 independent experiments using GraphPad Prism 9.4.0. Error bars represent SEM. VC: Vehicle control.

µM had no significant impact on cell proliferation at 24 h and 48 h (Figure 1C). Hence the aforementioned IC$_{50}$ value (5.0 µm) and half its IC$_{50}$ (2.5 µm) were selected for downstream experiments.

BZD9L1 reduced SIRT1, SIRT2, intercellular adhesion molecule 1, integrin-alpha V and vascular endothelial cadherin genes in Ea.HY926 cells

As BZD9L1 is a small molecule inhibitor with SIRT1 and 2 inhibitory activities, Ea.HY926 cells were treated with non-killing doses of BZD9L1 at 2.5 µM and 5.0 µM to investigate its repressive effects on SIRT 1 and SIRT 2. SIRT 1 and 2 gene expression were significantly reduced in cells treated with BZD9L1 at 2.5 µM and 5.0 µM, compared to the negative control (Figure 2A). BZD9L1 also significantly down-regulated intercellular adhesion molecule 1 (ICAM-1), integrin-alpha V (ITGA5) and vascular endothelial cadherin (VE-cadherin) cell adhesion molecules (Figure 2B) compared to the negative control.

BZD9L1 induced apoptotic cell death and arrested Ea HY926 cells at the G1 phase

The live, necrotic, early apoptotic, and late apoptotic fractions and cell cycle distribution of cells were detected by Annexin V and PI staining at 72 h post-treatment. Cells treated with BZD91 at 2.5 µM and 5.0 µM showed a significant increase in early and late apoptosis compared to the negative control (Figure 3A). BZD9L1 at 2.5 µM and 5.0 µM induced cell cycle arrest at the G1 phase compared to the negative control group (Figure 3B).

BZD9L1 hampered Ea.HY926 EC spheroid and mouse choroid sprouting

BZD9L1 at 2.5 µM and 5.0 µM significantly reduced Ea.HY926 EC spheroid sprouting compared to negative control 72 h post-treatment (Figure 3C). Considering the native tissue and microenvironmental factor, BZD9L1 employed at higher concentrations of 10 µM, and 20 µM decreased the sprouting area in mouse choroids compared to the negative control 96 h post-treatment (Figure 4A). Interestingly, BZD9L1 at both concentrations also regressed sproutings of mouse choroids 24 h post-treatment of sprouted choroids (Figure 4B). ALK1 inhibited both the sprouting and regression processes in mouse
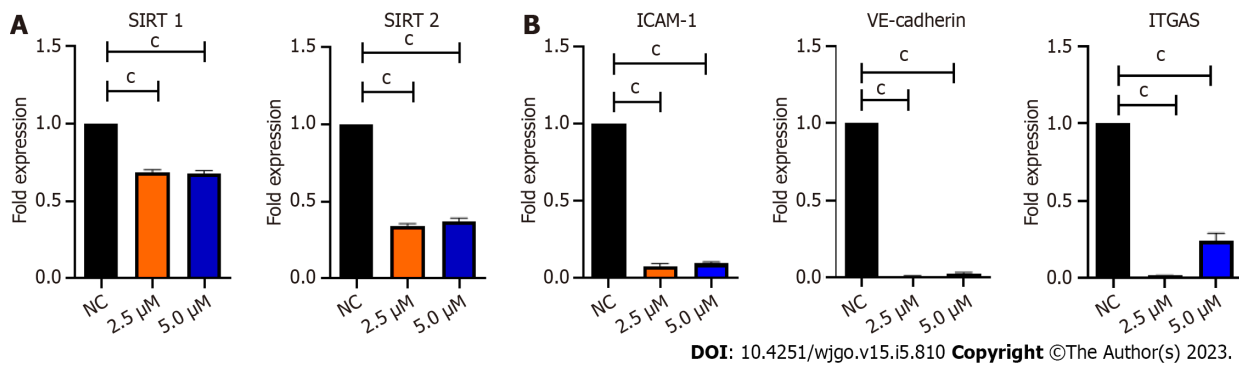
Figure 2 Quantitative polymerase chain reaction analysis of Ea.HY926 cells treated with BZD9L1 for 4 h. A: BZD9L1 reduced the gene expression levels of sirtuin 1 (SIRT1) and SIRT 2; B: Intercellular adhesion molecule 1 (ICAM-1), vascular endothelial cadherin (VE-cadherin) and integrin-alpha V (ITGA5) cell adhesion markers including ICAM-1, VE-cadherin and ITGA5, compared to the negative control (NC). Statistical analysis ($^{c}P < 0.001$), one-way ANOVA with Bonferroni posthoc test, $n = 3$ independent experiments using GraphPad Prism 9.4.0. Error bars represent SEM. SIRT: Sirtuin; ICAM-1: Intercellular adhesion molecule 1; NC: Negative control; VE-cadherin: Vascular endothelial cadherin; ITGA5: Integrin-alpha V.

choroids.

Conditioned media from BZD9L1-treated ECs reduced CRC spheroid invasion

Co-culture models are widely utilized to examine how physical contact between cells and autocrine and/or paracrine interactions affect cell activity. An indirect co-culture was performed to determine the effects of BZD9L1 on EC and CRC spheroids. The 48-h post-treatment conditioned media from Ea.HY926 cells were used to treat CRC spheroids to study the tumor-EC relationship. Analysis of the EC-conditioned media revealed that BZD9L1 at 5 μM diminished Angiogenin (A), bFGF (B), PDGF-BB (C), and PIGF (D) levels compared to the negative control group (Figure 5A). The other six cytokines were either not expressed at basal levels or below the detection limit. The conditioned media from all treatment groups significantly reduced the invasion of the CRC spheroids relative to the negative control group (Figure 5B).

BZD9L1 inhibited colorectal tumor growth and angiogenesis in the xenograft model

Sunitinib at 40 mg/kg and BZD9L1 inhibited tumor growth in low- (50 mg/kg) and high- (250 mg/kg) dose groups compared to the vehicle group (Figure 6A). Notably, the tumor growth in high-dose-treated mice was significantly impeded compared to the low-dose-treated mice group. The 250 mg/kg BZD9L1-treated xenograft tumor growth was equally inhibited to the same level as the 40 mg/kg Sunitinib positive control-treated mice. The weight of the tumor also decreased with the increasing doses of BZD9L1 (Figure 6B). There was no change in the body weight in all treatment groups compared to the vehicle control group except for the Sunitinib-treated group (Figure 6C). BZD9L1 (50 mg/kg) did not significantly reduce tumor necrosis compared to vehicle control Figure 6D. However, only BZD9L1 (250 mg/kg) and Sunitinib positive control significantly inhibited tumor necrosis compared to the vehicle control group. In addition, BZD9L1 at low and high doses significantly reduced Ki67 protein expression in tumor tissue compared to vehicle control Figure 6E. qPCR analyses of the xenograft tumors revealed no significant change in murine SIRT1 (mSIRT1) but a down-regulation of mSIRT2 in BZD9L1-treated groups at both 50 mg/kg and 250 mg/kg, compared to the vehicle control group (Figure 7A). In addition, BZD9L1 at 250 mg/kg reduced hSIRT1 and hSIRT2 gene expression in mice, compared to the vehicle control group. Although BZD9L1 at the low dose did not significantly reduce cluster of differentiation 31 (CD31) gene expression compared to the vehicle control, BZD9L1 at high doses decreased both CD31 and CD34 gene expression compared to the vehicle control (Figure 7B).

DISCUSSION

The fundamental stages of sprouting angiogenesis comprise enzymatic degradation of the EC basement membrane, followed by EC proliferation, migration, tube formation in response to growth factors gradient and finally, mural cell stabilization. Despite the emergence of novel targeted therapies targeting cancer cells or the tumor vasculature, the development of small molecule inhibitors to treat CRC to arrest the two main features of CRC, namely uncontrollable malignant cell proliferation and angiogenesis simultaneously, remain a potential avenue to be explored. The anticancer and SIRT 1 and 2 inhibitory activities of BZD9L1 have previously been established[5]. The human EC line Ea.HY926 was chosen for this study because it is continuous, exhibits various characteristics common to vascular ECs, and is frequently employed as an *in vitro* model for angiogenesis[15,16]. Despite the reduction of EC
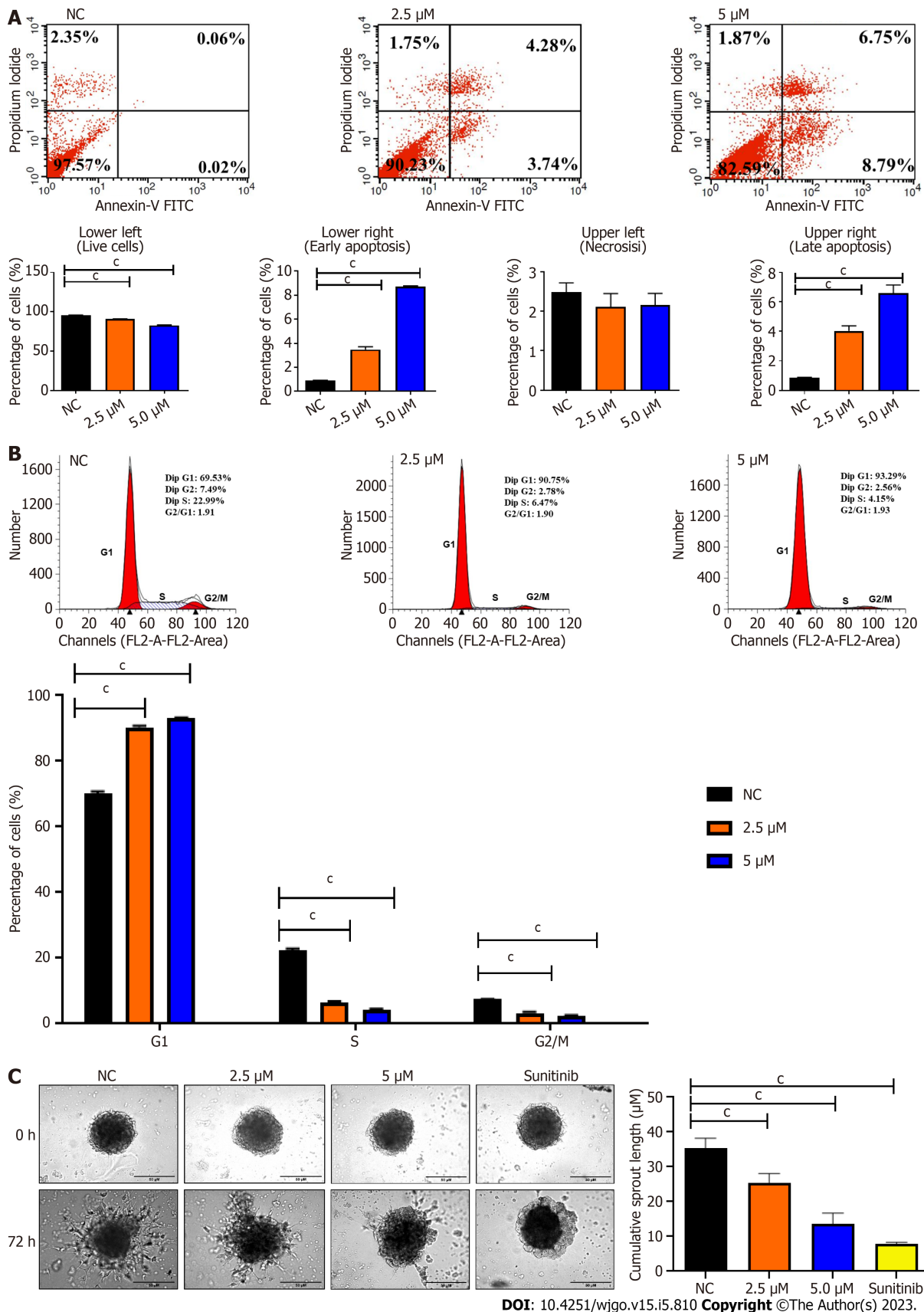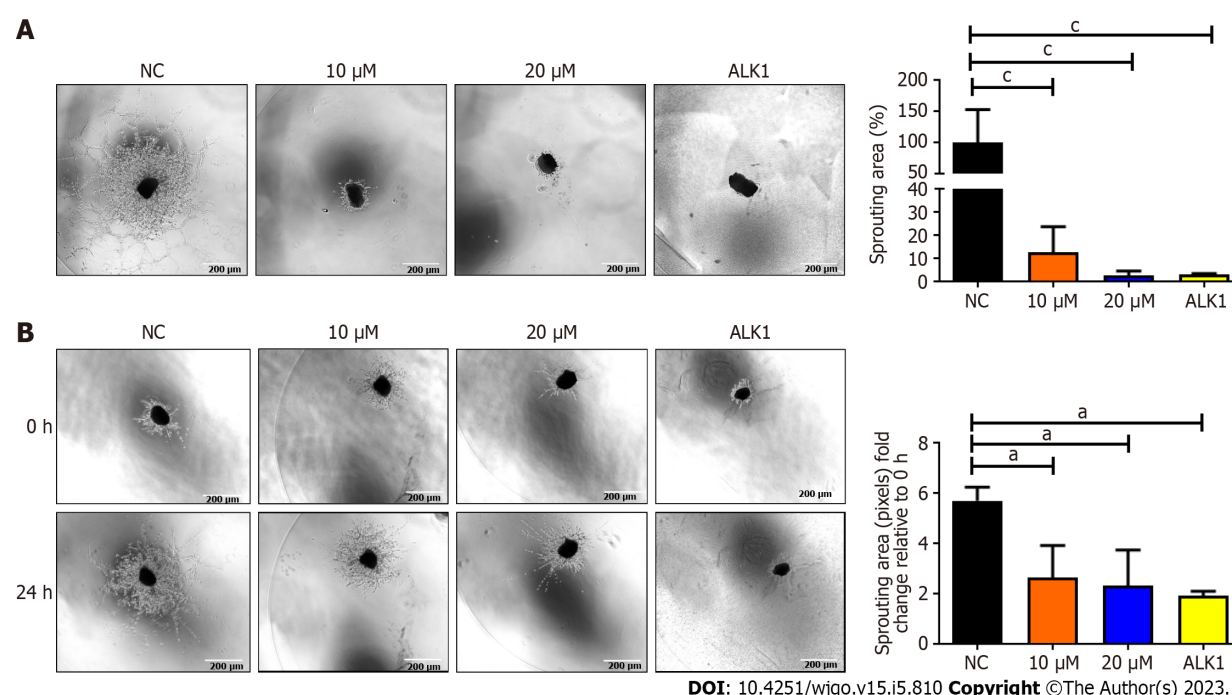
Figure 3 Representative cytograms and endothelial cells sprouting spheroids depict the negative impact of BZD9L1 on endothelial cell functions. A: BZD9L1 at 2.5 μM and 5.0 μM induced apoptosis; B: Cell cycle arrest at G1 phase; C: But reduced Ea.Hy 926 spheroid sprouting compared to the negative control at 72 h. Sunitinib anti-angiogenic agent was used as the positive control. Statistical analysis ($^{c}P < 0.001$), one-way ANOVA with Bonferroni posthoc test, n = 3 independent experiments using GraphPad Prism 9.4.0. Error bars represent SEM. NC: Negative control.

DOI: 10.4251/wjgo.v15.i5.810 **Copyright** ©The Author(s) 2023.

DOI: 10.4251/wjgo.v15.i5.810 **Copyright** ©The Author(s) 2023.

Figure 4 Analyses of mouse choroidal endothelial sprouts in sprouting and regression models. A: BZD9L1 impeded mouse choroidal endothelial sprouting 96 h post-treatment; B: Regressed choroid sprouting 24 h post-treatment compared to the negative control. A receptor like type 1 anti-angiogenic agent was used as the positive control regression and sprouting assays. Statistical analysis ([a]$P < 0.05$; [c]$P < 0.001$), one-way ANOVA with Bonferroni posthoc test, $n = 2$ independent experiments using GraphPad Prism 9.4.0. Error bars represent SEM. ALK1: A receptor like type 1; NC: Negative control.
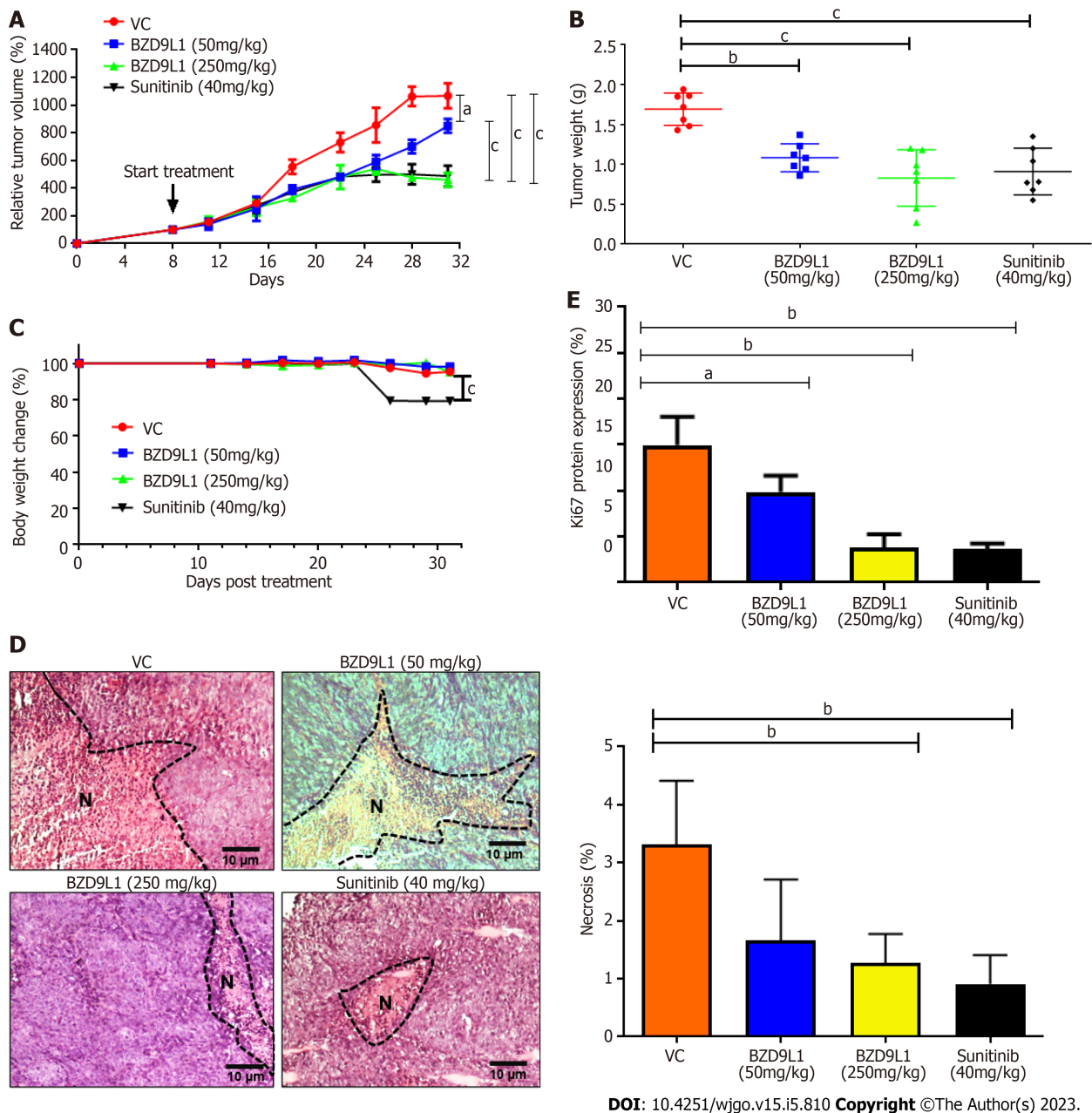

DOI: 10.4251/wjgo.v15.i5.810 **Copyright** ©The Author(s) 2023.
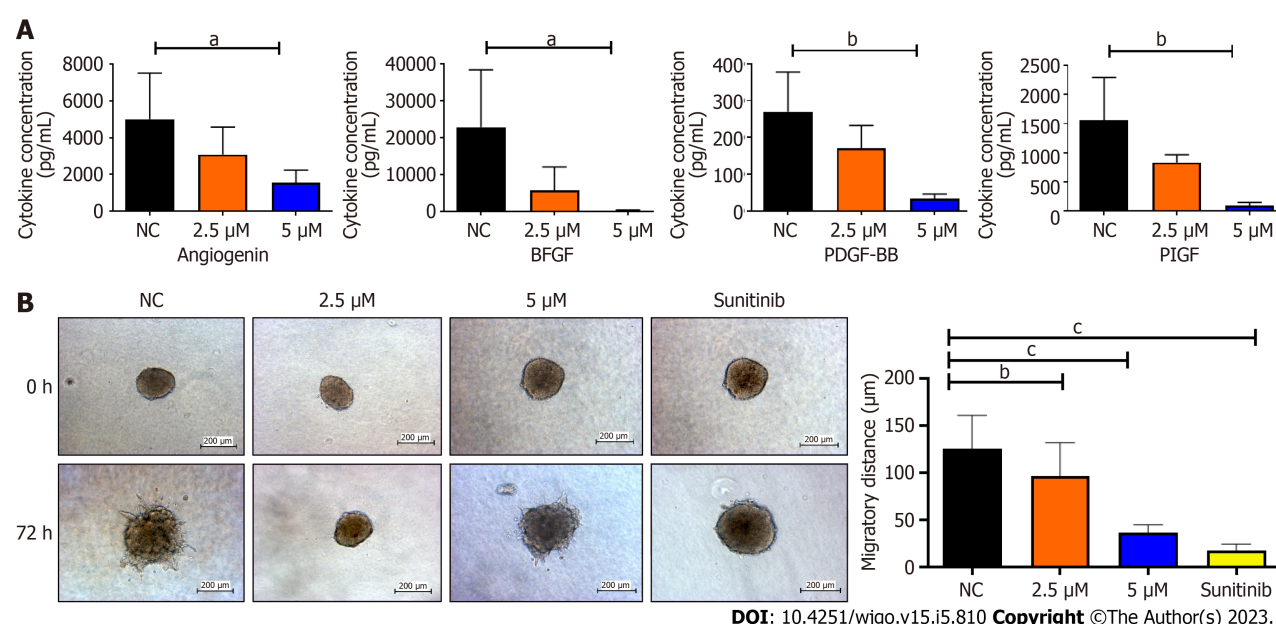
Figure 5 Refreshed conditioned media from Ea.Hy 926 endothelial cells 48 h post-treatment with Sunitinib positive control, BZD9L1 at 2.5 μM, 5.0 μM, or negative control for 48 h prior, were subjected to Quantibody Human Angiogenesis array and indirect co-culture with HCT116 colorectal cancer spheroids. A: BZD9L1 at 5 μM down-regulated angiogenin, fibroblast growth factor, platelet-derived growth factor and placental growth factor cytokine concentrations in Ea.Hy 926 conditioned media; B: The endothelial conditioned media from BZD9L1 or sunitinib positive control-treated groups impeded HCT116 tumor invasion at 72 h. Statistical analysis ([a]$P < 0.05$; [b]$P < 0.01$; [c]$P < 0.001$), one-way ANOVA with Bonferroni posthoc test, $n = 2$ independent experiments for protein array analysis and $n = 3$ independent replicates for co-culture analysis using GraphPad Prism 9.4.0. Error bars represent SEM. NC: Negative control. bFGF: Fibroblast growth factor; PDGF-BB: Platelet-derived growth factor; PIGF: Placental growth factor; NC: Negative control.

adhesive capability at double the IC$_{50}$ of BZD9L1 (10 μM) compared to the negative control at 5 h (Figure 1B), the implicated dose was non-toxic, as revealed by the mean cell index of the EC at early point (Figure 1C). The downregulation of ICAM-1, VE-cadherin and ITGA5 cell adhesion molecules post BZD9L1 treatment in Ea HY926 highlights its potential to inhibit the early steps of angiogenesis.

Figure 6 Tumor growth analyses of HCT116 tumor xenograft in nude mice. Treatments were administered when the tumors reached 100 mm³. A: Relative tumor volume; B: Tumor weight and; C: Percentage body weight change in mice treated with vehicle control (0.5% carboxymethylcellulose), BZD9L1 (50 mg/kg per 3 d, BZD9L1 (250 mg/kg per 3 d) and sunitinib (40 mg/kg per 3 d) as the positive control; D: Tumor necrosis percentage in sections stained with haematoxylin and eosin. N indicates necrotic tissues; E: Ki67 proliferation protein expression in treated and vehicle control groups. Statistical analysis ([a]$P < 0.05$; [b]$P < 0.01$; [c]$P < 0.001$). The non-linear fit was used to track the tumor size and body weight change over time, one-way ANOVA with Bonferroni posthoc test for tumor weight, $n = 6$ animals per group) using GraphPad Prism 9.4.0. Error bars represent SEM. VC: Vehicle control.

The effect of BZD9L1 on a panel of cell adhesion molecules and their post-translational modifications may be crucial to determine the specific mechanisms that may impact EC adhesion stability and function, thus warrants further investigations.

Cell viability is influenced by cell proliferation and cell death. During angiogenesis, ECs exhibit an increased proliferation rate. Cell proliferation is important in the elongation and maturation of new blood vessels. BZD9L1 at all doses reduced the mean cell index (indicative of cell viability or proliferation) of EC at 72 h when compared to the negative control. Nevertheless, a significant decrease in cell index was only noted in EC treated with 10 μM BZD9L1 at 48 h, which served as the basis for proceeding with downstream molecular assays using half the IC$_{50}$ (2.5 μM) and IC$_{50}$ (5.0 μM) BZD9L1. BZD9L1 at the tested doses significantly induced apoptosis and arrested EC at the G1 phase (Figure 3A and B), which suggests that BZD9L1 reduced EC viability by triggering apoptotic cell death and inhibiting cell cycle progression. The G1 phase is where cells prepare to divide. If cells cannot carry out DNA repair at G1 cell cycle arrest, they will enter the apoptosis stage. Cells commit suicide during the
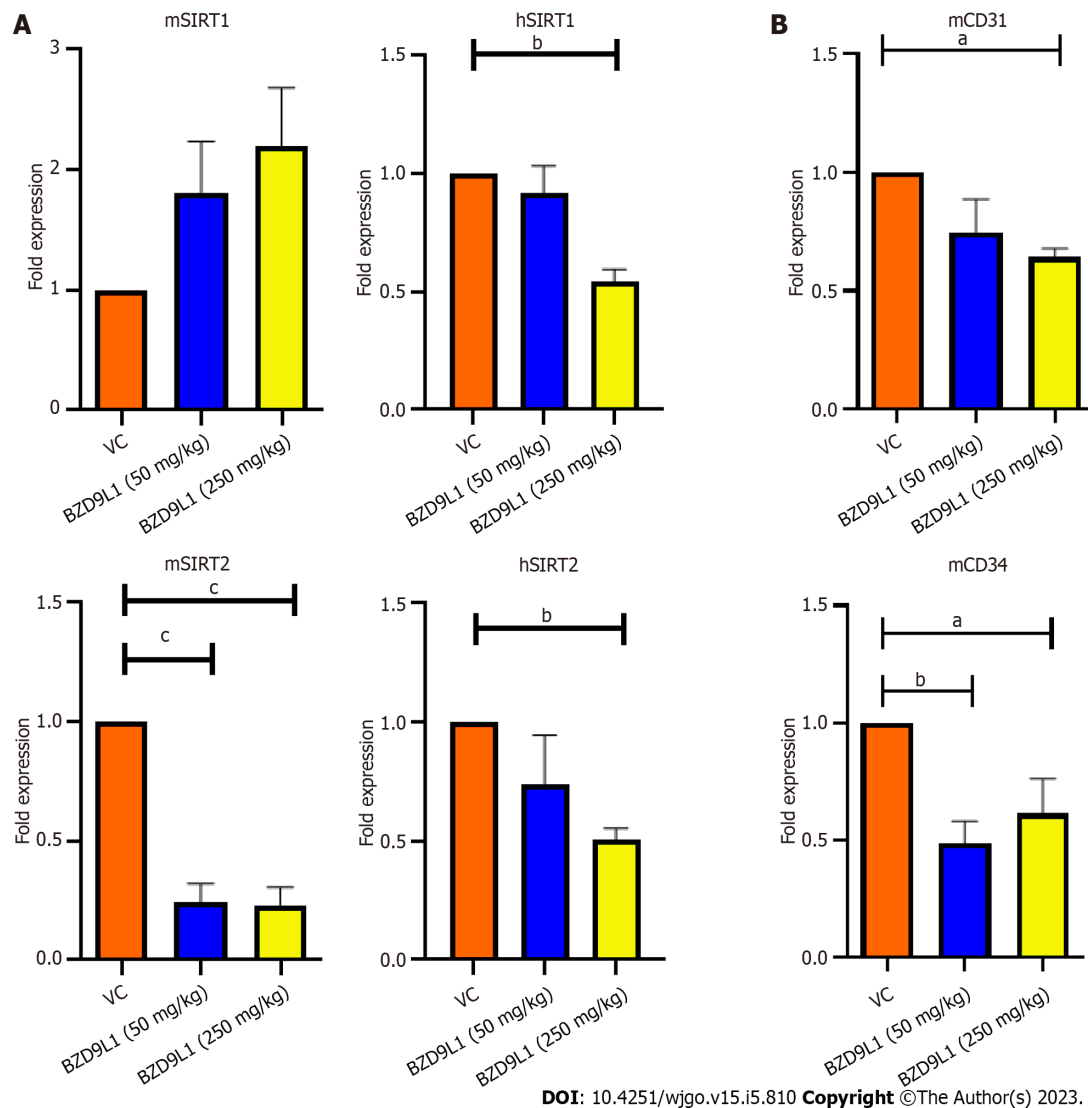
Figure 7 Quantitative polymerase chain reaction analyses of murine SIRT1, mSIRT2 and endothelial cell markers in HCT116 tumor xenograft in nude mice. A: BZD9L1 did not significantly affect murine SIRT1 (mSIRT1) gene expression in the colorectal cancer xenograft tumors but down-regulated mSIRT2 at low (50 mg/kg) and high (250 mg/kg) doses and reduced human SIRT1 (hSIRT1) and hSIRT2 gene expression at 250 mg/kg, compared to vehicle control; B: BZD9L1 at the high dose significantly reduced cluster of differentiation 31 (CD31) gene expression. Both low and high doses of BZD9L1 decreased mCD34 gene expression compared to vehicle control. Statistical analysis [a]$P < 0.05$; [b]$P < 0.01$; [c]$P < 0.001$), one-way ANOVA with Bonferroni posthoc test, $n = 6$ animals per group) using GraphPad Prism 9.4.0. Error bars represent SEM. VC: Vehicle control.

process of cell apoptosis as a result of signals that start programmed cell death. Apoptosis is crucial for blood vessel regression during angiogenesis[17,18]. Correspondingly, BZD9L1 increased the percentage of apoptotic EC compared with the negative control group, which is corroborated by our previous report in CRC[6].

In a meta-analysis, elevated expression of SIRT1 in CRC is correlated with vascular invasion and inferior outcomes[19]. Meanwhile, increased SIRT2 expression was associated with poor prognosis in CRC patients and the inhibition of SIRT2 Limited CRC tumor angiogenesis *via* inactivation of the STAT3/VEGFA signaling pathway[20]. BZD9L1 downregulated the gene expression of SIRT1 and 2 in Ea.HY926 cells *in vitro* (Figure 2A). Endothelial cell proliferation, migration, and the assembling of vascular networks were reduced when SIRT1 and SIRT2 activities were blocked *in vitro*[20-22]. BZD9L1 at 250 mg/kg reduced the expression of hSIRT1 and hSIRT2 genes, highlighting the ability of BZD9L1 to modulate human SIRTs in HCT116 xenograft tumours which collectively led to the inhibition of tumor growth. However, mSIRT2 but not mSIRT1 was significantly downregulated by BZD9L1 *in vivo* (Figure 7A). BZD9L1 was previously reported to display a higher affinity for SIRT2 than SIRT1[5], which may explain this observation. Furthermore, the tumor microenvironment may play a role in therapeutic response. SIRT1 and SIRT2 are also expressed in other stromal cells, and their interplay may regulate tumor immune responses that impact CRC progression[23,24].

SIRT 1 and SIRT 2 inhibition have been shown to suppress EC proliferation, migration and angiogenesis[25,26]. In human retinal microvascular ECs, SIRT1 downregulation prevented EC

migration and tube formation, whereas SIRT1 overexpression had the opposite effects[26]. The SIRT2 inhibitor, AK-1, dramatically reduced the ability of human umbilical vein ECs (HUVECs) to form tubes [27]. EC spheroid (Figure 3C) and choroidal sprouting (Figure 4A) were shown to be negatively affected by BZD9L1 in an increasing dose. In addition, the compound also regressed sprouting choroids compared to the negative control (Figure 4B). A recent study proved that when sprouting angiogenesis occurs, the vascular endothelium expresses SIRT1 in high levels, and inhibiting SIRT1 function prevents the development and migration of endothelial sprouts as well as the *in vitro* construction of a primitive vascular network[21]. Furthermore, a study on primary murine lung ECs exhibited that when the chemotactic response was muted, tube development was attenuated, and the length of the EC spheroid sprout was shorter in cells lacking SIRT1[28]. Furthermore, SIRT2 knockdown in HUVECs diminished its angiogenic potential, while overexpression of SIRT2 Led to contrasting outcomes[29]. Altogether, these findings highlighted that BZD9L1 negatively regulated SIRT 1 and SIRT 2 to reduce EC viability, adhesion and sprouting.

The EC-conditioned media treated with BZD9L1 at 5 µM portrayed angiogenin, bFGF, PDGF-BB, and PIGF to be significantly reduced compared to the negative control (Figure 5A). Several studies have previously reported angiogenin being essential in EC proliferation that can promote the development of new blood vessels[30,31]. Angiogenin was also shown to stimulate progenitor cell proliferation and protect the stemness of primitive hematopoietic stem/progenitor cells, which suggests that its downregulation may negatively regulate angiogenesis *via* BZD9L1 inhibitory effects. bFGF can impact the upregulation of VEGF directly and promote EC proliferation[32]. The ECs secrete PDGF-BB that binds to PDGFR-β on the mural cells, which then affects the formation and maturation of new capillaries. PlGF also positively regulates angiogenesis; thus, its inhibition reduces EC growth, migration, and survival [33]. Therefore, the downregulation of these cytokines in BZD9L1-treated EC at 5 µM may collectively impede the steps of angiogenesis and HCT116 CRC invasion through paracrine signalling in the co-culture model, while at 2.5 µM, BZD9L1 may potentially reduce CRC invasion through the regulation of other growth factors that were not captured by the protein array (Figure 5B).

BZD9L1 was previously reported to have anti-tumor effects in CRC xenograft models when used in adjunct with 5-Fluorouracil[7]. BZD9L1 did not lead to any acute or repeated dose toxicity symptoms, and neither were there any cellular or molecular changes that would be considered significantly and biologically toxic[10]. In this study, BZD9L1 significantly inhibited the progression of CRC tumor xenograft models. Although the body weight of mice treated with BZD9L1 remained unaffected compared to the vehicle control group, the weight of the mice treated with sunitinib declined treatment, as also confirmed by other studies supporting the weight loss potential of sunitinib in mice by targeting fat cells, leading to appetite loss[34,35]. The mechanisms of weight loss due to sunitinib treatment are poorly understood.

Tumor necrosis is linked to poor prognosis and overall survival of CRC patients[36]. Therefore, the reduction of tumor necrosis in mice treated with 250 mg/kg BZD9L1 further underlines the therapeutic potential of this benzimidazole analogue. On the other hand, Ki67 protein expression was significantly reduced in all treatment groups compared to the vehicle control group, indicating the possibility of BZD9L1 to reduce tumor growth to be *via* the impediment of tumor proliferation. In this study, the amount of vessels left post-treatment were determined *via* gene expression analyses of mCD31 and mCD34, due to the high necrotic nature of the tumors which limited the accurate interpretation of immunohistochemical staining (Figure 7B). BZD9L1 at a high dose significantly reduced mCD31 gene expression compared to the vehicle control group, while both low and high doses of the compound decreased mCD34 gene levels. This may be due to the expression profile of CD31 and CD34, which are not limited strictly to just EC but also a subset of leukocytes and/or hematopoietic progenitor cells that express the CD31 and CD34 antigens, respectively. In addition, gene expression may not positively correlate to protein expression levels due to the turnover rate and possible post-translational modification. Despite this, anti-CD31 and CD34 antibodies are often employed as a diagnostic for vascular malignancies and are highly sensitive indicators of EC differentiation[37,38].

Pathophysiological angiogenesis is mediated by the VEGR which correlates with increased microvessels density and metastatic spread in CRC[39]. Clinical studies showed that resistance developed against angiogenesis inhibitor in single-agent anti-angiogenic therapy. Research has demonstrated the blockage of the VEGF pathway to normalise the tumour-associated vessels. As tumour vasculature matures, angiogenesis inhibitor temporarily reduces tumour hypoxia by improving targeted therapy's efficacy to ensure delivery of oxygen or cytotoxic or cytostatic drugs to the tumour sites[40]. However, the normalisation of tumour vascular usually occurs only transiently at the initial time of anti-angiogenic therapy. Hypoxia increases with prolonged VEGF inhibition due to vessel pruning, which consecutively induces systemic secretion of other pro-angiogenic cytokines[41].

The failure of anti-angiogenic monotherapy may be attributed to the induction of VEGF-independent compensatory mechanisms. The activation of other angiogenic signaling pathways may also induce the expression of other pro-angiogenic cytokines instead of VEGF[42]. Therefore, the development of new inhibitors that target other molecules that are involved in the angiogenesis signaling pathway may be essential. In our study, BZD9L1 did not significantly affect VEGF expression. Hence the compound may be a potential candidate to be employed as an adjunct to VEGF inhibitors or chemotherapy in CRC, as previously reported[7]. Besides, anti-angiogenic therapy combined with chemotherapy or immune

checkpoint inhibitors has demonstrated promising therapeutic effects with enhanced clinical benefits for cancer patients[43]. As such, small molecule inhibitors with anti-angiogenic and anti-cancer capabilities, such as that portrayed by BZD9L1, could be a promising new strategy for cancer therapy by targeting the two distinct features of CRC.

CONCLUSION

BZD9L1 hindered the processes of angiogenesis in EC through the down-regulation of cell adhesion molecules, SIRT1 and SIRT2 genes. Similarly, the angiogenesis array displayed a depletion of angiogenesis cytokines angiogenin, bFGF, PDGF-BB and PIGF in BZD9L1-treated ECs. Furthermore, BZD9L1 arrested the cells at the G1 phase and induced apoptosis in EC. These results suggest that BZD9L1 displayed cytotoxic and cytostatic properties to negatively regulate the formation of new blood vessels. The sprouting potential and the sprout regression were also noted in mouse choroid tissues post-treatment. Moreover, the indirect co-culture assay demonstrated that BZD9L1 could reduce CRC spheroid invasion compared to the negative control. This result potentially suggests that suppression of angiogenesis may obstruct cancer cell progression, as further confirmed *in vivo*. In mice, BZD9L1 had the ability to retard HCT116 colorectal xenograft tumor growth. In relation to this, the tumor necrosis and Ki67 protein expression percentage in the tumor sections were reduced in the BZD9L1-treated groups compared to vehicle control. CD31 and CD34 protein expressions were not evaluated due to the limitation posed by necrosis in the tumor sections. However, gene analyses revealed a decline in these well-reported EC markers in BZD9L1-treated mice.

Overall, this project has provided insights into the potential of BZD9L1 to reduce EC growth and progression *in vitro* and hinder CRC tumor growth *in vivo*. It is noteworthy that this study should be recapitulated using at least one other primary ECs or ECs derived from CRC to confirm the findings. Moreover, BZD9L1 may regulate other angiogenesis players and cancer pathways to impact cancer progression, as suggested in a recent study where 58 other BZD9L1-regulated targets were identified [44]. *In vivo* study in an orthotopic model where the tumor cells will be engrafted into the organ, which matches the cancer cell type may also provide a more realistic model to study the mechanism of action of BZD9L1 and its impact on the tumor microenvironment. Additionally, real-time vessel perfusion imaging may be performed to more accurately assess the efficacy of BZD9L1 treatment[45]. This study provides valuable insights into BZD9L1 as a potential anti-angiogenic agent in CRC.

ARTICLE HIGHLIGHTS

Research background

The growth and spread of colorectal cancer (CRC) are highly dependent on angiogenesis. Epigenetic regulation of the genes in endothelial cells (ECs) in the vicinity of tumor cells plays a vital role in tumor angiogenesis. Sirtuins are class III histone deacetylase enzymes that are implicated in angiogenesis. Their potential roles in cancer have stimulated investigation to seek potent and selective sirtuin (SIRT) inhibitors, potentially leading to new therapeutic breakthroughs. BZD9L1 is a reported small molecule inhibitor with anticancer activities. However, its potential as an anti-angiogenic agent has not been explored.

Research motivation

A patient's prognosis and survival rate remain heterogenous for which tumor attributes, dynamic host response factors, and treatment quality may be accountable. Some CRC patients become resilient to these anti-angiogenic drugs and standard therapies such as chemotherapy and radiation. Hence, this work opens a new avenue for the establishment of a potential novel anti-angiogenic agent through sirtuin inhibition in tumor angiogenesis.

Research objectives

To determine the anti-angiogenic activity of BZD9L1 benzimidazole analogue in CRC.

Research methods

The *in vitro* experiments comprise cell viability, adhesion. spheroid sprouting, quantitative polymerase chain reaction (qPCR), angiogenesis protein array, cell cycle and apoptosis analyses *via* flow cytometry and indirect co-culture. Mouse choroids were employed to assess the negative impact of BZD9L1 on sprouting and vessel regression. HCT116 CRC cells were injected subcutaneously into athymic nude mice and treated with vehicle control or BZD9L1 at 50 mg/kg and 250 mg/kg. Hematoxylin and eosin staining was performed to determine the percentage of necrosis in the tumor section. Finally, immuno-histochemistry and qPCR were conducted to investigate the expression of Ki67 protein and murine

CD34/ CD31 as well as SIRT1 and SIRT2, respectively.

Research results
Findings from this study highlighted the ability of BZD9L1 to inhibit EC functions in *in vitro*, *ex vivo* and co-culture models. Additionally, BZD9L1 retarded tumor growth *in vivo* compared to the vehicle control group. Overall, the findings underscore the potential of BZD9L1 to treat CRC.

Research conclusions
BZD9L1 impeded angiogenesis in ECs, mouse choroid tissues and the CRC xenograft model. This study provides valuable insights into BZD9L1 as a potential anti-angiogenic agent in CRC.

Research perspectives
Findings from this study may provide the basis for BZD9L1 benzimidazole analogue as a targeted therapy for the treatment of CRC.

ACKNOWLEDGEMENTS

FOOTNOTES

ORCID number: Chern Ein Oon 0000-0002-4685-6408; Gurjeet Kaur 0000-0002-6232-5703.

REFERENCES

1   **Saif MW**, Elfiky A, Salem RR. Gastrointestinal perforation due to bevacizumab in colorectal cancer. *Ann Surg Oncol* 2007; **14**: 1860-1869 [PMID: 17356952 DOI: 10.1245/s10434-006-9337-9]

2   **Komazin G**, Ptak RG, Emmer BT, Townsend LB, Drach JC. Resistance of human cytomegalovirus to D- and L-ribosyl benzimidazoles as a tool to identify potential targets for antiviral drugs. *Nucleosides Nucleotides Nucleic Acids* 2003; **22**: 1725-1727 [PMID: 14565505 DOI: 10.1081/NCN-120023123]

3   **Pieroni M**, Tipparaju SK, Lun S, Song Y, Sturm AW, Bishai WR, Kozikowski AP. Pyrido[1,2-a]benzimidazole-based agents active against tuberculosis (TB), multidrug-resistant (MDR) TB and extensively drug-resistant (XDR) TB. *ChemMedChem* 2011; **6**: 334-342 [PMID: 21259445 DOI: 10.1002/cmdc.201000490]

4   **Napper AD**, Hixon J, McDonagh T, Keavey K, Pons JF, Barker J, Yau WT, Amouzegh P, Flegg A, Hamelin E, Thomas RJ, Kates M, Jones S, Navia MA, Saunders JO, DiStefano PS, Curtis R. Discovery of indoles as potent and selective inhibitors of the deacetylase SIRT1. *J Med Chem* 2005; **48**: 8045-8054 [PMID: 16335928 DOI: 10.1021/jm050522v]

5   **Yoon Y**, Ali M, Wei A, Choon T, Oon C, Shirazi A, Parang K. Correction: discovery of a potent and highly fluorescent sirtuin inhibitor. *Medchemcomm* 2015; **6**: 2235 [DOI: 10.1039/C5MD90057C]

6   **Tan YJ**, Lee YT, Yeong KY, Petersen SH, Kono K, Tan SC, Oon CE. Anticancer activities of a benzimidazole compound through sirtuin inhibition in colorectal cancer. *Future Med Chem* 2018; **10**: 2039-2057 [PMID: 30066578 DOI: 10.4155/fmc-2018-0052]

7   **Tan YJ**, Lee YT, Petersen SH, Kaur G, Kono K, Tan SC, Majid AMSA, Oon CE. BZD9L1 sirtuin inhibitor as a potential adjuvant for sensitization of colorectal cancer cells to 5-fluorouracil. *Ther Adv Med Oncol* 2019; **11**: 1758835919878977 [PMID: 31632470 DOI: 10.1177/1758835919878977]

8   **Cabebe E**, Wakelee H. Sunitinib: a newly approved small-molecule inhibitor of angiogenesis. *Drugs Today (Barc)* 2006; **42**: 387-398 [PMID: 16845442 DOI: 10.1358/dot.2006.42.6.985633]

9   **Cunha SI**, Pietras K. ALK1 as an emerging target for antiangiogenic therapy of cancer. *Blood* 2011; **117**: 6999-7006 [PMID: 21467543 DOI: 10.1182/blood-2011-01-330142]

10   **Lee YT**, Tan YJ, Mok PY, Kaur G, Sreenivasan S, Falasca M, Oon CE. Sex-divergent expression of cytochrome P450 and SIRTUIN 1-7 proteins in toxicity evaluation of a benzimidazole-derived epigenetic modulator in mice. *Toxicol Appl Pharmacol* 2022; **445**: 116039 [PMID: 35489524 DOI: 10.1016/j.taap.2022.116039]

11   **Oon CE**, Bridges E, Sheldon H, Sainson RCA, Jubb A, Turley H, Leek R, Buffa F, Harris AL, Li JL. Role of Delta-like 4 in Jagged1-induced tumour angiogenesis and tumour growth. *Oncotarget* 2017; **8**: 40115-40131 [PMID: 28445154 DOI: 10.18632/oncotarget.16969]

12   **Shao Z**, Friedlander M, Hurst CG, Cui Z, Pei DT, Evans LP, Juan AM, Tahiri H, Duhamel F, Chen J, Sapieha P, Chemtob S, Joyal JS, Smith LE. Choroid sprouting assay: an ex vivo model of microvascular angiogenesis. *PLoS One* 2013; **8**: e69552 [PMID: 23922736 DOI: 10.1371/journal.pone.0069552]

13   **Qiu B**, Tan A, Tan YZ, Chen QY, Luesch H, Wang X. Largazole Inhibits Ocular Angiogenesis by Modulating the Expression of VEGFR2 and p21. *Mar Drugs* 2021; **19** [PMID: 34436310 DOI: 10.3390/md19080471]

14   **Voce P**, D'Agostino M, Moretti S, Sponziello M, Rhoden K, Calcinaro F, Tamburrano G, Tallini G, Puxeddu E, Filetti S, Russo D, Durante C. Sunitinib inhibits tumor vascularity and growth but does not affect Akt and ERK phosphorylation in xenograft tumors. *Oncol Rep* 2011; **26**: 1075-1080 [PMID: 21850379 DOI: 10.3892/or.2011.1422]

15   **Edgell CJ**, McDonald CC, Graham JB. Permanent cell line expressing human factor VIII-related antigen established by hybridization. *Proc Natl Acad Sci U S A* 1983; **80**: 3734-3737 [PMID: 6407019 DOI: 10.1073/pnas.80.12.3734]

16   **Bauer J**, Margolis M, Schreiner C, Edgell CJ, Azizkhan J, Lazarowski E, Juliano RL. In vitro model of angiogenesis using a human endothelium-derived permanent cell line: contributions of induced gene expression, G-proteins, and integrins. *J Cell Physiol* 1992; **153**: 437-449 [PMID: 1280276 DOI: 10.1002/jcp.1041530302]

17   **Dimmeler S**, Zeiher AM. Endothelial cell apoptosis in angiogenesis and vessel regression. *Circ Res* 2000; **87**: 434-439 [PMID: 10988233 DOI: 10.1161/01.res.87.6.434]

18   **Chavakis E**, Dimmeler S. Regulation of endothelial cell survival and apoptosis during angiogenesis. *Arterioscler Thromb Vasc Biol* 2002; **22**: 887-893 [PMID: 12067894 DOI: 10.1161/01.atv.0000017728.55907.a9]

19   **Hong WG**, Pyo JS. The clinicopathological significance of SIRT1 expression in colon cancer: An immunohistochemical study and meta-analysis. *Pathol Res Pract* 2018; **214**: 1550-1555 [PMID: 30082156 DOI: 10.1016/j.prp.2018.07.022]

20   **Hu F**, Sun X, Li G, Wu Q, Chen Y, Yang X, Luo X, Hu J, Wang G. Inhibition of SIRT2 limits tumour angiogenesis *via* inactivation of the STAT3/VEGFA signalling pathway. *Cell Death Dis* 2018; **10**: 9 [PMID: 30584257 DOI: 10.1038/s41419-018-1260-z]

21   **Potente M**, Ghaeni L, Baldessari D, Mostoslavsky R, Rossig L, Dequiedt F, Haendeler J, Mione M, Dejana E, Alt FW, Zeiher AM, Dimmeler S. SIRT1 controls endothelial angiogenic functions during vascular growth. *Genes Dev* 2007; **21**: 2644-2658 [PMID: 17938244 DOI: 10.1101/gad.435107]

22   **Edatt L**, Poyyakkara A, Raji GR, Ramachandran V, Shankar SS, Kumar VBS. Role of Sirtuins in Tumor Angiogenesis. *Front Oncol* 2019; **9**: 1516 [PMID: 32010617 DOI: 10.3389/fonc.2019.01516]

23   **Fang H**, Huang Y, Luo Y, Tang J, Yu M, Zhang Y, Zhong M. SIRT1 induces the accumulation of TAMs at colorectal cancer tumor sites *via* the CXCR4/CXCL12 axis. *Cell Immunol* 2022; **371**: 104458 [PMID: 34847407 DOI: 10.1016/j.cellimm.2021.104458]

24   **Jiang C**, Liu J, Guo M, Gao X, Wu X, Bai N, Guo W, Li N, Yi F, Cheng R, Xu H, Zhou T, Jiang B, Sun T, Wei S, Cao L. The NAD-dependent deacetylase SIRT2 regulates T cell differentiation involved in tumor immune response. *Int J Biol Sci* 2020; **16**: 3075-3084 [PMID: 33061819 DOI: 10.7150/ijbs.49735]

25   **Gao Z**, Wang H, Xiao FJ, Shi XF, Zhang YK, Xu QQ, Zhang XY, Ha XQ, Wang LS. SIRT1 mediates Sphk1/S1P-induced proliferation and migration of endothelial cells. *Int J Biochem Cell Biol* 2016; **74**: 152-160 [PMID: 26923291 DOI: 10.1016/j.biocel.2016.02.018]

26   **Lin Y**, Li L, Liu J, Zhao X, Ye J, Reinach PS, Qu J, Yan D. SIRT1 Deletion Impairs Retinal Endothelial Cell Migration Through Downregulation of VEGF-A/VEGFR-2 and MMP14. *Invest Ophthalmol Vis Sci* 2018; **59**: 5431-5440 [PMID:

30452596 DOI: 10.1167/iovs.17-23558]

27   **Jung SY**, Kim CM, Kim DY, Lee DH, Lee KS, Kwon S-M. The Role of Sirtuin-2 in Tubular Forming Activity of Human Umbilical Vein Endothelial Cells. *J Life Sci* 2013; **23**: 131-136 [DOI: 10.5352/JLS.2013.23.1.131]

28   **Das A**, Huang GX, Bonkowski MS, Longchamp A, Li C, Schultz MB, Kim LJ, Osborne B, Joshi S, Lu Y, Treviño-Villarreal JH, Kang MJ, Hung TT, Lee B, Williams EO, Igarashi M, Mitchell JR, Wu LE, Turner N, Arany Z, Guarente L, Sinclair DA. Impairment of an Endothelial NAD(+)-H(2)S Signaling Network Is a Reversible Cause of Vascular Aging. *Cell* 2018; **173**: 74-89.e20 [PMID: 29570999 DOI: 10.1016/j.cell.2018.02.008]

29   **Tang Y**, Jin G, Zhang B, Chen K. SIRT2 is down-regulated in myocardial infarction mice and regulates reparative angiogenesis *via* targeting AKT signaling pathway. *Int J Cli Exp Med* 2017; **10**: 11820-11827

30   **Hu G**, Riordan JF, Vallee BL. Angiogenin promotes invasiveness of cultured endothelial cells by stimulation of cell-associated proteolytic activities. *Proc Natl Acad Sci U S A* 1994; **91**: 12096-12100 [PMID: 7991590 DOI: 10.1073/pnas.91.25.12096]

31   **Kim BS**, Kim JS, Yang SS, Kim HW, Lim HJ, Lee J. Angiogenin-loaded fibrin/bone powder composite scaffold for vascularized bone regeneration. *Biomater Res* 2015; **19**: 18 [PMID: 26331087 DOI: 10.1186/s40824-015-0040-4]

32   **Stavri GT**, Zachary IC, Baskerville PA, Martin JF, Erusalimsky JD. Basic fibroblast growth factor upregulates the expression of vascular endothelial growth factor in vascular smooth muscle cells. Synergistic interaction with hypoxia. *Circulation* 1995; **92**: 11-14 [PMID: 7788904 DOI: 10.1161/01.CIR.92.1.11]

33   **Xiang L**, Varshney R, Rashdan NA, Shaw JH, Lloyd PG. Placenta growth factor and vascular endothelial growth factor a have differential, cell-type specific patterns of expression in vascular cells. *Microcirculation* 2014; **21**: 368-379 [PMID: 24410720 DOI: 10.1111/micc.12113]

34   **Kumar RM**, Arlt MJ, Kuzmanov A, Born W, Fuchs B. Sunitinib malate (SU-11248) reduces tumour burden and lung metastasis in an intratibial human xenograft osteosarcoma mouse model. *Am J Cancer Res* 2015; **5**: 2156-2168 [PMID: 26328246]

35   **Tanaka Y**, Shibata MA, Morimoto J, Otsuki Y. Sunitinib suppresses tumor growth and metastases in a highly metastatic mouse mammary cancer model. *Anticancer Res* 2011; **31**: 1225-1234 [PMID: 21508369]

36   **Väyrynen SA**, Väyrynen JP, Klintrup K, Mäkelä J, Karttunen TJ, Tuomisto A, Mäkinen MJ. Clinical impact and network of determinants of tumour necrosis in colorectal cancer. *Br J Cancer* 2016; **114**: 1334-1342 [PMID: 27195424 DOI: 10.1038/bjc.2016.128]

37   **Vieira SC**, Silva BB, Pinto GA, Vassallo J, Moraes NG, Santana JO, Santos LG, Carvasan GA, Zeferino LC. CD34 as a marker for evaluating angiogenesis in cervical cancer. *Pathol Res Pract* 2005; **201**: 313-318 [PMID: 15991838 DOI: 10.1016/j.prp.2005.01.010]

38   **Baumann CI**, Bailey AS, Li W, Ferkowicz MJ, Yoder MC, Fleming WH. PECAM-1 is expressed on hematopoietic stem cells throughout ontogeny and identifies a population of erythroid progenitors. *Blood* 2004; **104**: 1010-1016 [PMID: 15126319 DOI: 10.1182/blood-2004-03-0989]

39   **Lopes-Coelho F**, Martins F, Pereira SA, Serpa J. Anti-Angiogenic Therapy: Current Challenges and Future Perspectives. *Int J Mol Sci* 2021; **22** [PMID: 33916438 DOI: 10.3390/ijms22073765]

40   **Jain RK**. Normalizing tumor vasculature with anti-angiogenic therapy: a new paradigm for combination therapy. *Nat Med* 2001; **7**: 987-989 [PMID: 11533692 DOI: 10.1038/nm0901-987]

41   **Ribatti D**, Annese T, Ruggieri S, Tamma R, Crivellato E. Limitations of Anti-Angiogenic Treatment of Tumors. *Transl Oncol* 2019; **12**: 981-986 [PMID: 31121490 DOI: 10.1016/j.tranon.2019.04.022]

42   **Gacche RN**. Compensatory angiogenesis and tumor refractoriness. *Oncogenesis* 2015; **4**: e153 [PMID: 26029827 DOI: 10.1038/oncsis.2015.14]

43   **Song Y**, Fu Y, Xie Q, Zhu B, Wang J, Zhang B. Anti-angiogenic Agents in Combination With Immune Checkpoint Inhibitors: A Promising Strategy for Cancer Treatment. *Front Immunol* 2020; **11**: 1956 [PMID: 32983126 DOI: 10.3389/fimmu.2020.01956]

44   **Tan YJ**, Lee YT, Mancera RL, Oon CE. BZD9L1 sirtuin inhibitor: Identification of key molecular targets and their biological functions in HCT 116 colorectal cancer cells. *Life Sci* 2021; **284**: 119747 [PMID: 34171380 DOI: 10.1016/j.lfs.2021.119747]

45   **Porter TR**, Xie F, Silver M, Kricsfeld D, Oleary E. Real-time perfusion imaging with low mechanical index pulse inversion Doppler imaging. *J Am Coll Cardiol* 2001; **37**: 748-753 [PMID: 11693747 DOI: 10.1016/s0735-1097(00)01204-3]